Eur. Phys. J. B **3**, 507–515 (1998)

THE EUROPEAN PHYSICAL JOURNAL B

The smooth structural change in mesoscopic Peierls chains

I. Bâldea[a], H. Köppel, and L.S. Cederbaum

Theoretische Chemie, Physikalisch-Chemisches Institut, Universität Heidelberg, Im Neuenheimer Feld 253, 69120 Heidelberg, Germany

Received: 3 January 1998 / Revised: 13 March 1998 / Accepted: 3 April 1998

Abstract. We investigate the Peierls transition in finite chains by exact (Lanczos) diagonalization and within a seminumerical method based on the factorization of the electron-phonon wave function (Adiabatic Ansatz, AA). AA can be applied for mesoscopic chains up to micrometer sizes and its reliability can be checked self-consistently. Our study demonstrates the important role played for finite systems by the tunneling in the double well potential. The chains are dimerized only if their size N exceeds a critical value N_c which increases with increasing phonon frequency. Quantum phonon fluctuations yield a broad transition region. This *smooth* Peierls transition contrasts not only to the sharp mean field transition, but also with the sharp RPA soft mode instability, although RPA partially accounts for quantum phonon fluctuations. For weak coupling the dimerization disappears below micrometer sizes; therefore, this effect could be detected experimentally in mesoscopic systems.

PACS. 63.22.+m Phonons in low-dimensional structures and small particles – 63.20.-e Phonons in crystal lattices – 71.45.Lr Charge-density-wave systems

1 Introduction

Although a variety of mesoscopic systems attract an increasing interest at present [1], experimental studies on quasi-one-dimensional materials exhibiting a Peierls-CDW transition are practically absent so far (CDW: Charge Density Wave). The only exception we know is an investigation on blue bronzes [2], where the strong size-dependence of the electronic gap we have recently predicted [3] seems to be confirmed, and several other intriguing features were observed. In the attempt to fill the gap between the conventional fields of solid state physics and quantum chemistry of molecules the understanding of mesoscopic Peierls-CDW systems is particularly important. Theoretically, it is necessary to develop a method suitable for such systems. In infinite solids the Mean-Field (MF) approach often represents a useful approximation to identify ground state orderings. Treatments beyond MF include quantum phonon fluctuations in one-dimensional electron-phonon models within approximate many-body techniques, *e.g.* one-loop expansions [4] or variational ansätze [5]. None of these methods is appropriate to study structural changes in mesoscopic systems. If they predict a structural transformation, it is always *sharp*. This prediction is unphysical in *finite* systems. On the other side, exact treatments by means of the Monte-Carlo method [6] and numerical diagonalization [3,7] are possible only for small chains. For strong couplings, exact results obtained on small chains can easily be extrapolated for infinite systems.

For the presently considered Peierls chain, the strong coupling limit is less interesting since the fast approach to the thermodynamical limit masks specific properties of mesoscopic systems. Throughout this paper, emphasis is on weaker couplings when the quantum fluctuations play an important part and the thermodynamical limit is approached sufficiently slowly. This has been demonstrated by our recent study of mesoscopic chains ($N \sim 100-1000$) [3]. There, we developed an approximate method based on the full numerical diagonalization in the Hilbert subspace of wave functions expressed as a product of electronic and phonon wave functions. This will be referred to as the Adiabatic Ansatz (AA), avoiding an ambiguous "adiabatic" name used for technically inequivalent approximations. The advantage of AA is considerable, particularly when electron-electron interactions can be neglected. Requiring both small computer memory and computing time, it can be applied up to mesoscopic sizes. For periodic chains with $N = 4n$ (n is an integer) we showed that AA is reliable in parameter regions well beyond the textbook claim on "adiabatic" approximations and its accuracy can be tested by calculations done within AA [3].

We report in this paper detailed results on ground state properties of finite Peierls chains at half filling. Several more recent studies on Hubbard models [8] rediscovered a fact known since long in chemistry [9]: periodic chains with $N = 4n + 2$ sites have properties that differ from those with $N = 4n$. We have also found a difference

[a] e-mail: ioan@tc.pci.uni-heidelberg.de

between the cases $N = 4n$ and $N = 4n + 2$ when considering the lattice motion of Peierls periodic chains. It is due to the fact that the lowest excitation energy for free electrons is zero in the former case but finite ($4t\sin(\pi/N)$, t — hopping integral) in the latter. In this paper we shall restrict ourselves to periodic chains with $N = 4n+2$ sites. The following could be mentioned to motivate this choice. Essential for the aforementioned difference is the gap at the Fermi level of free electrons. An on-site electron repulsion yields a finite gap at the Fermi level in both cases. This makes the periodic chains with $N = 4n$ sites resembling those with $N = 4n + 2$ [8]. One could also mention that $4n$-site rings are rather exotic in molecular physics.

The main *physical* result of this paper is to demonstrate why and how the Peierls transition in finite chains qualitatively differs from that in infinite chains. We find that only systems that are large enough are dimerized; smaller ones are normal, and the transition between normal and dimerized regimes is *smooth*. Even at relatively small phonon frequencies the critical size required for dimerization is considerable larger than the MF estimate because of quantum phonon fluctuations. For electron-phonon couplings that are relatively weak, the critical sizes fall in the micrometer range. Therefore, this effect could be experimentally detected in mesoscopic systems. So, with the present study an answer can be given to a fundamental question: how small can a *dimerized* system be? To the best of authors' knowledge, neither the answer nor the question could be found in the literature. Long ago, a similar question has been addressed for superconductors[10] and for bond alternating cyclic polyenes (annulenes) [9].

The main *technical* result of the present work is to show that AA represents a useful method for studying periodic chains with $N = 4n+2$. This is a nontrivial generalization of the similar result of reference [3] for periodic chains with $N = 4n$. A separate check of the AA method is necessary for $N = 4n + 2$, because the adiabatic potential curves have an appearance that differs from those for $N = 4n$. To do this we shall use the direct comparison with the exact (Lanczos) diagonalization for small chains and examine diagonal corrections [3] for mesoscopic ones. Besides, the present study provides an explanation why conventional many-body theories have a very limited applicability to finite dimerized systems.

The remaining part of the paper is organized as follows. The model is defined in Section 2 and the analytical methods are presented in Section 3. The methods of numerical diagonalization are exposed in Section 4. Results for small chains, obtained by exact diagonalization and within AA, on the ground state as well as lowest lattice excitations are reported in Section 5. Section 6 is devoted to mesoscopic systems. Section 7 summarizes the results.

2 Model

We shall investigate periodic chains with $N = 4n+2$ sites and N spin-1/2 electrons. By setting the lattice constant to unity, the Fermi wave vector is given by $k_F = \pi/2$. The chosen half-filling case is of physical interest and simplifies the numerical effort: there is a single $+2k_F$-phonon mode in this problem ($4k_F = 2\pi$). The model Hamiltonian has the form:

$$\begin{aligned} H &= H_{el} + H^0_{ph};\\ H^0_{ph} &= \Omega_0 a^\dagger a = \frac{\Omega_0}{2}\left(Q - \frac{\partial}{\partial Q}\right)\left(Q + \frac{\partial}{\partial Q}\right),\\ H_{el} &= H^0_{el} + H_{el-ph} = \sum_{s,p}\Big[\epsilon_p\left(c^\dagger_{1,p,s}c_{1,p,s} - c^\dagger_{2,p,s}c_{2,p,s}\right)\\ &\quad + gQ\sqrt{2/N}\left(c^\dagger_{1,p,s}c_{2,p,s} + c^\dagger_{2,p,s}c_{1,p,s}\right)\Big], \end{aligned} \tag{1}$$

where label 1 (2) refers to right (left)-moving electrons, $\epsilon_p = 2t\sin(2\pi p/N)$, a ($a^\dagger$) is the annihilation (creation) operator of the $2k_F$-phonon of frequency Ω_0, and $Q = (a + a^\dagger)/\sqrt{2}$. The electron-phonon coupling strength used below is $\lambda = 2g^2/(\pi t\Omega_0)$. In all p-summations p runs over the set of half-integers $-N/4,\ \cdots, N/4-1$. The transformation $Q \to -Q$ and, *e.g.* $c_{j,p,s} \to (-1)^j c_{j,p,s}$ ($j = 1, 2$), leaves the Hamiltonian (1) invariant.

3 Analytical methods

Problems similar to (1) have been often solved by using various approximations which exploit the difference between electronic and ionic inertia and are generically called "adiabatic". The most simple of them is to consider a frozen classical lattice, *i.e.* $H^0_{ph} \simeq V_{ph}(Q) \equiv \Omega_0 Q^2/2$. The corresponding wave functions and energies depend parametrically on Q and can immediately be found, because equations (1) now becomes diagonalizable:

$$\begin{aligned} H_A(Q) &= H_{el} + V_{ph}(Q)\\ &= \sum_{p,s}\omega_p(Q)\left(\tilde{c}^\dagger_{2,p,s}\tilde{c}_{2,p,s} - \tilde{c}^\dagger_{1,p,s}\tilde{c}_{1,p,s}\right) + \Omega_0 Q^2/2. \end{aligned} \tag{2}$$

Here $\tilde{c}_{1,p,s} = u_p c_{1,p,s} - v_p c_{2,p,s}$, $\tilde{c}_{2,p,s} = v_p c_{1,p,s} + u_p c_{2,p,s}$, $(u_p, v_p) = \sqrt{(1 \pm \epsilon_p/\omega_p)/2}$, $\omega_p = \sqrt{\epsilon_p^2 + \Delta^2}$ and $\Delta = g|Q|\sqrt{2/N}$. The picture thus emerging is that of a system (the well-known Peierls semiconductor) with two electronic bands $\pm\omega_p(Q)$ [11]. In the ground state, the lower (upper) band is completely occupied (empty): $|\Phi_0(Q)\rangle = \prod_{ps}\tilde{c}^\dagger_{1,p,s}|0\rangle$ ($|0\rangle$ — vacuum). By minimizing the corresponding adiabatic potential,

$$\begin{aligned} V_0(Q) &\equiv \langle\Phi_0(Q)|H_A(Q)|\Phi_0(Q)\rangle\\ &= -2\sum_p \omega_p(Q) + \Omega_0 Q^2/2, \end{aligned}$$

one gets $\pm Q = \mathcal{Q}_{MF}(\geq 0)$. The MF gap $2\Delta_{MF} = 2g\mathcal{Q}_{MF}\sqrt{2/N} \approx 16t\exp(-1/\lambda)$ is different from the electronic gap $2[4t^2\sin^2(\pi/N) + \Delta^2_{MF}]^{1/2}$ because of the finite

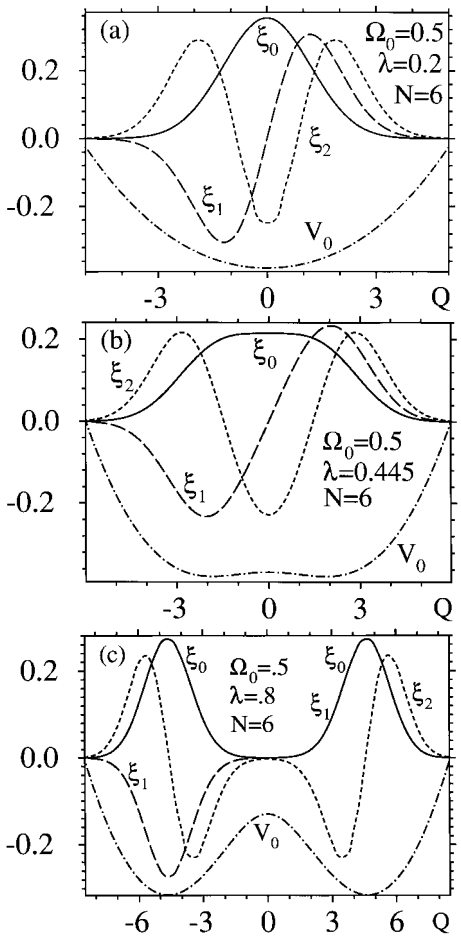

Fig. 1. The adiabatic potential $V_0(Q)$ (in arbitrary units) and the lowest phononic eigenstates $\xi_{0,1,2}(Q)$ computed within AA in the ground electronic state for 6-site chains.

gap of the free electron spectrum. A nonvanishing distortion ($\mathcal{Q}_{MF} > 0$) occurs only above the critical coupling λ_c^{MF} given by: $N/\lambda_c^{MF} = 2\pi t \sum_p 1/|\epsilon_p|$ [12]. Adiabatic curves $V_0(Q)$ are shown in Figures 1. In the dimerized chain ($\lambda > \lambda_c^{MF}$), the ions are displaced from their original positions l by $(-1)^l \mathcal{Q}_{MF}$ (l is an integer).

The crudest way to incorporate the phonon dynamics is to factorize the total wave function $|\Psi_{CAA}, \pm\rangle = |\Phi_0(\pm\,\mathcal{Q}_{MF})\rangle|\tilde{\xi}_\pm\rangle$ using the electronic wave function $|\Phi_0(\pm\,\mathcal{Q}_{MF})\rangle$ at the MF geometry. $|\Phi_{CAA,\pm}\rangle$ is an eigenstate of the MF Hamiltonian $H_A(\pm\,\mathcal{Q}_{MF})$. In the spirit of the previous nomenclature [13], we shall call this the Crude Adiabatic Ansatz (CAA). In the CAA Hilbert subspace, the original Hamiltonian (1) is equivalent to:

$$H_{CAA}(\pm\,\mathcal{Q}_{MF}) = H_A(\pm\,\mathcal{Q}_{MF}) + \Omega_0 b^\dagger b,$$

where $b = a \mp \mathcal{Q}_{MF}/\sqrt{2}$ corresponds to phonons in the dimerized lattice. $|\tilde{\xi}_\pm\rangle$ describes harmonic oscillations around $\pm\,\mathcal{Q}_{MF}$ with the bare frequency Ω_0.

A renormalization of the phonon frequency Ω can be obtained only by retaining the quantum electron-phonon interaction. Within the Random Phase Approximation (RPA) in the dimerized state ($\lambda > \lambda_c^{MF}$) one gets:

$$\frac{\Omega^2}{\lambda\Omega_0^2} = \frac{2\pi t}{N}\sum_p \frac{1}{\sqrt{\epsilon_p^2 + \Delta_{MF}^2}} \frac{\Delta_{MF}^2 - \Omega^2/4}{\epsilon_p^2 + \Delta_{MF}^2 - \Omega^2/4}$$
$$\equiv \frac{1}{\lambda} + \Pi(\Omega). \tag{3}$$

In the normal state ($\lambda < \lambda_c^{MF}$), the above polarization should be replaced by:

$$\Pi_N(\Omega) = -\frac{2\pi t}{N}\sum_p \frac{|\epsilon_p|}{\epsilon_p^2 - \Omega^2/4}\,. \tag{4}$$

4 Numerical methods

4.1 Adiabatic Ansatz (AA)

The electronic and phononic problems can be separated if the total wave function is factorized, $|\Psi_\nu^\delta\rangle = |\Phi_\delta(Q)\rangle|\xi_\nu^\delta\rangle$. Here, $|\Phi_\delta(Q)\rangle = \prod_{p,s} \tilde{c}^\dagger_{j_{p,s},p,s}|0\rangle$ ($j_{p,s} = 1,2$) are eigenstates of the Hamiltonian (2) describing noninteracting quasi-electrons at fixed lattice geometry Q. Each $|\Phi_\delta(Q)\rangle$ generates an adiabatic potential $V_\delta(Q) = \langle\Phi_\delta(Q)|H_A(Q)|\Phi_\delta(Q)\rangle$. By neglecting the nonadiabatic coupling matrix elements $\Gamma_{\delta,\delta'} \equiv 2\langle\Phi_\delta(Q)|\partial/\partial Q|\Phi_{\delta'}(Q)\rangle\partial/\partial Q + \langle\Phi_\delta(Q)|\partial^2/\partial Q^2|\Phi_{\delta'}(Q)\rangle$ [14] one gets an approximate phononic eigenvalue problem (AA without diagonal corrections):

$$\left[V_\delta(Q) + \Omega_0(a^\dagger a - Q^2/2)\right]|\xi_\nu^\delta\rangle = E_{\delta,\nu}|\xi_\nu^\delta\rangle. \tag{5}$$

Equation (5) is nontrivial but can be solved numerically in the Q-representation. The discrete eigenvalues of Q represent the counterpart of the discrete points that should be used by numerical quadratures in the occupation number representation [3]. Within AA, the phonon dynamics is determined by the adiabatic potential $V_\delta(Q)$.

The AA quantum motion occurs on *isolated* adiabatic surfaces but, in reality, a coupling between various surfaces exists ($\Gamma_{\delta,\delta'} \neq 0$). $\Gamma_{\delta,\delta'}$ becomes large or singular only when adiabatic surfaces come close or touch each other [14]. For small N and $\Omega_0 \lesssim t$, AA is accurate: the minimum energy separation $4t\sin(\pi/N)$ of $V_0(Q)$ from other adiabatic surfaces yields $\Gamma_{\delta,\delta'} \simeq 0$. The direct comparison with exact results (Sect. 5) confirms this conclusion. This argument holds no more for mesoscopic systems, because the energy separation becomes smaller than Ω_0. There, however, one can show that the diagonal elements of Γ are larger than the off-diagonal ones [19]. Therefore, the parameter ranges beyond which AA breaks down can be determined self-consistently from the point where the diagonal corrections [3] computed within AA become large.

If a distortion exists, the AA quantum motion proceeds in the double well potential $V_0(Q) = V_0(-Q)$. Since it is one dimensional, the AA ground state is nondegenerate. Let us denote the three lowest eigenvalues (eigenvectors) of equation (5) by E_A, $E_A + \Omega_{1,A}$ and $E_A + \Omega_{2,A}$ ($|\xi_{0,1,2}\rangle$),

respectively. For large λ and/or small Ω_0, $\Omega_{1,A}$ represents a tunneling splitting; it is small and the next eigenstate is well separated energetically ($\Omega_{2,A} \gg \Omega_{1,A}$).

In addition to the energies obtained without diagonal corrections and specified by A, we shall also employ energies with diagonal corrections, specified by the subscript a: $E_a \equiv \langle\xi_0|\langle\Phi_0(Q)|H|\Phi_0(Q)\rangle|\xi_0\rangle$ and $E_a + \Omega_{j,a} \equiv \langle\xi_j|\langle\Phi_0(Q)|H|\Phi_0(Q)\rangle|\xi_j\rangle$ ($j = 1, 2$). The difference between them will be used to characterize the accuracy of AA.

4.2 Exact Lanczos diagonalization

For a fixed number of basis functions in phonon number representation (increased progressively, until reaching convergence), and including all $\binom{2N}{N}$ multielectronic configurations, we have applied the Lanczos algorithm to the Hamiltonian (1) to compute the exact eigenvalues $E_e < E_e + \Omega_{1,e} < E_e + \Omega_{2,e}$ and eigenvectors $|\mathcal{G}_e\rangle$, $|\Psi_{1,e}\rangle$ and $|\Psi_{2,e}\rangle$ of the ground state and the two lowest energy lattice excitations. If $V_0(Q)$ possesses two deep minima, the tunnel splitting $\Omega_{1,e}$ is small the usual method (see Ref. [3] and references cited therein) fails to determine $\Omega_{1,e}$ and $|\Psi_{1,e}\rangle$. Then, to resolve the quasi-degeneracy the Lanczos algorithm was repeated with a starting Lanczos vector orthogonal to $|\mathcal{G}_e\rangle$. The lowest energy Ritz vector $|\Psi_{1,e}\rangle$ obtained in the second step corresponds to the eigenstate which is quasi-degenerate with the ground state: their energy difference $\Omega_{1,e}$ represents the tunneling splitting.

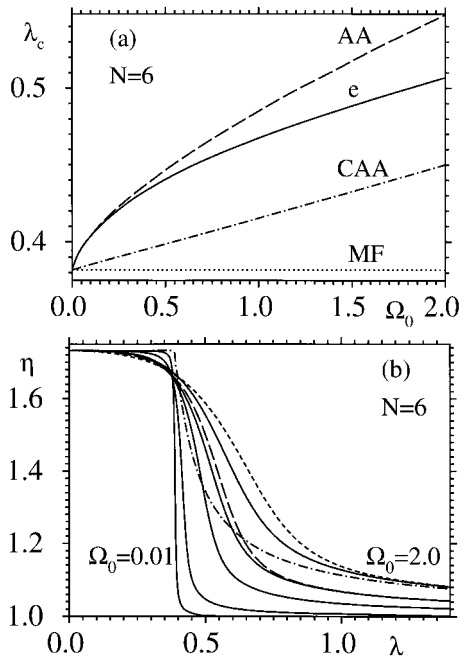

Fig. 2. Results on the gradual Peierls transition for 6-site chains. (a) Curves of the critical coupling λ_c obtained by exact diagonalization (index e), within AA, MF and CAA. (b) λ-dependence of η for $\Omega_0 = 0.01; 0.1; 0.5; 1.0; 2.0$ (increasing upwards for large λ). Within drawing accuracy, the AA-curves (dashed lines) can be distinguished from the exact ones (solid lines) only for $\Omega_0 = 1.0$ (long dash) and 2.0 (short dash). The dot-dashed curve is the CAA result for $\Omega_0 = 2.0$.

5 Exact and approximate results for small systems

We have studied in detail chains with 6 and 10 sites. Since no notable difference between them was observed, we shall only present results for 6-site chains, investigated in a very broad range of parameters ($0.001 < \lambda < 2$, $0.01 < \Omega_0 < 20$). In all numerical results we set $t = 1$.

5.1 Lowest energy wave functions and the smooth Peierls transition

Conventional many-body approaches are only able to compute averaged properties of a system. The methods exposed in Section 4 provide the richest information on the physics of the Peierls transition, that contained in the wave functions. Within AA one can directly inspect $\xi(Q)$. The exact diagonalization allows one to get the contribution of various lattice geometries to a certain eigenstate $|\Psi\rangle$ by computing the probability distribution $P(Q) \equiv \sum_\delta |\langle\delta, Q|\Psi\rangle|^2$ (δ runs over all multielectronic configurations) [15].

MF predicts a stabilization of a twofold degenerate dimerized state for a coupling stronger than $\lambda_c^{MF} (= 0.382$ for $N = 6)$ and a normal state otherwise (*cf.* Sect. 3). Figure 1 shows how realistic the MF-description is. At the moderately small frequency $\Omega_0 = 0.5$, the differences between exact diagonalization and AA are small for all computed quantities. Therefore, only AA results on $\xi_{0,1,2}(Q)$ (*cf.* Sect. 4.1) will be presented below.

The ground state $\xi_0(Q)$ possesses a single maximum at $Q = 0$ for weak coupling and two symmetric maxima for strong coupling. A critical coupling $\lambda_c(\Omega_0)$ will be defined by the point separating the two situations, referred to as the normal and dimerized regimes, respectively. The difference between $\lambda_c(\Omega_0)$ and λ_c^{MF} is an effect of quantum phonon fluctuations: $\lim_{\Omega_0 \to 0} \lambda_c(\Omega_0) = \lambda_c^{MF}$ (Fig. 2a). Quantum phonon fluctuations alter quantitatively and qualitatively the MF-CAA picture.

Unlike the CAA-picture, a notable phonon anharmonicity exists even in the normal regime. The stronger the coupling, the more pronounced is the anharmonicity. At $\lambda = 0.2$, the wave functions $\xi_{0,1,2}(Q)$ shown in Figure 1a do not qualitatively differ from those of a harmonic oscillator. Several numerical values given below show quantitative differences from those (given in parentheses) corresponding to the CAA-harmonic oscillator. $\xi_0(Q)$ has a FWHM-value of 2.82 (2.35) and $\xi_1(Q)$ possesses two symmetric extrema at $Q = \pm 1.19$ ($Q = \pm 0.707$). The minimum of $\xi_2(Q)$ at $Q = 0$ has an amplitude smaller than the symmetric $\xi_2(Q)$-maxima at $Q = \pm 1.88$ ($Q = \pm 1.58$) by a factor 1.151 (1.146).

With increasing λ the anharmonicity becomes more significant: $\xi_{0,1,2}(Q)$ become broader. For instance, at

$\lambda_c = 0.445$, the FWHM of $\xi_0(Q)$ is larger than for the CAA-harmonic oscillator by a factor 2.51.

At $\lambda = 0.8$, $\xi_0(Q)$ displays two maxima (*cf.* Fig. 1c) at $|Q_0| = 4.640$. The small difference to the MF-value $\mathcal{Q}_{MF} = 4.646$ demonstrates the small effect of quantum phonon fluctuations in the strong coupling limit. Within numerical accuracy either maximum is symmetric and has a FWHM of 2.54, corresponding to 2.35 for the CAA oscillations around $\pm\,\mathcal{Q}_{MF}$. $\xi_1(Q)$ behaves completely different from its counterpart of Figures 1a and b. To a very good approximation, one can consider ξ_0 and ξ_1 as the symmetric and antisymmetric superpositions of two functions centered on $\pm\,Q_0$, the counterpart of the CAA eigenvectors $|\tilde{\xi}_{\pm}\rangle$, respectively. This behavior is typical for molecular systems where the tunneling occurring in the adiabatic double well potential lifts the ground state degeneracy: the best known example is the NH_3 molecule [16]. Inspecting the region $Q < 0$ ($Q > 0$) of Figure 1c, one can see that $\xi_2(Q)$ has the appearance of a wave function describing an antisymmetric superposition of two states with single quanta describing harmonic oscillations around Q_0 and $-Q_0$. However, important quantitative differences exist. The maxima ($\pm\,Q_{max}$) of $\xi_2(Q)$ are closer to $\pm\,Q_0$ than its minima ($\pm\,Q_{min}$): $Q_{max} - Q_0 = 0.88$ and $Q_0 - Q_{min} = 1.14$. For CAA-harmonic oscillations both values are equal to 0.707. The value $|\,[max_Q \xi_2(Q)]\,/|\,[min_Q \xi_2(Q)] = 1.010$ is also different from harmonic oscillation value (1.146). This comparison demonstrates that, even for strong coupling, the physical description in terms of two CAA independent contributions of the wells at $\pm\,\mathcal{Q}_{MF}$ is poorer that one could claim from the small difference between Q_0 and $\mathcal{Q}_{MF}$. Approaching the value λ_c from above, the overlap between the two maxima of $\xi_0(Q)$ becomes more pronounced and the value of $\xi_0(Q)|_{Q=0}$ increases gradually. All aforementioned deviations from the CAA picture become more notable.

So, the above results demonstrate that one can essentially characterize the system as normal (dimerized) for weak (strong) coupling, but the transition between these regimes is gradual. The very broad critical region can be seen by inspecting (Fig. 2b) the quantity

$$\eta \equiv \langle Q^4 \rangle^{1/2} / \langle Q^2 \rangle .$$

At $\Omega_0 \to 0$ the CAA result is exact. For $\lambda < \lambda_c^{MF}$ one gets $\eta \to \sqrt{3}$, a value determined by zero point motion ($\mathcal{Q}_{MF} = 0$, $\langle Q^2 \rangle_0 = 1/2$, $\langle Q^4 \rangle_0 = 3/4$), while for $\lambda > \lambda_c^{MF}$, $\eta \to 1$ ($\mathcal{Q}_{MF} \propto \Delta_{MF}/\sqrt{\Omega_0} \to \infty$). The larger Ω_0, the stronger is the deviation of the $\eta(\lambda)$-curve from the CAA result: see the curves for $\Omega_0 = 2.0$ in Figure 2b.

The critical couplings deduced exactly (defined by means of the exact $P(Q)$) and within AA for $N = 6$ are shown in Figure 2a. Because the transition is smooth, a transition onset can only be defined by some suitable convention. The definition of $\lambda_c(\Omega_0)$ given above is a possible one with direct reference to the ground state wave function. Another possible definition is to use the ground state energy. The straightforward analysis reveals that the transition onset defined above is reasonably close to the point where $E_e + \Omega_0/2$ becomes equal to the local maximum of V_0 at $Q = 0$. For $\Omega_0 = 0.5$, this occurs at $\lambda = 0.461$. On the other side, the CAA zero point energy $\Omega_0/2$ becomes equal to the classical energy barrier $V_0(Q=0) - V_0(\mathcal{Q}_{MF})$ only at $\lambda = 0.508$. This analysis gives further insight into the physics of the transition. Basically, the enhancement of the critical coupling with respect to λ_c^{MF} is due to zero point motion, which causes a tunneling among the two minima at $\pm\,\mathcal{Q}_{MF}$. The critical coupling strength — 0.445 (AA) and 0.440 (exact diagonalization) at $\Omega_0 = 0.5$ — moves toward the MF value λ_c^{MF} as $\Omega_0 \to 0$ (Fig. 2a).

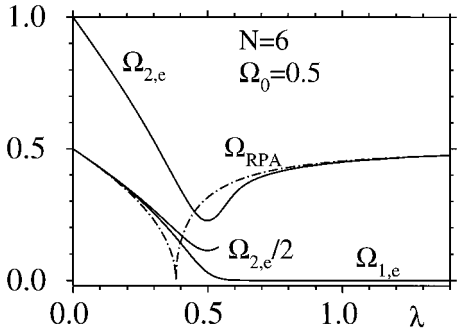

Fig. 3. Frequencies ($\Omega_{1,e}$ and $\Omega_{2,e}$) of the two lowest lattice excitations computed exactly and the dressed phonon frequency (Ω_{RPA}) obtained within RPA. For the chosen parameter values (inserted), exact and AA results are indistinguishable within drawing accuracy.

In summary, the quantum phonon fluctuations cause two main changes with respect to the MF predictions: (i) the exact ground state is nondegenerate, and (ii) for increasing coupling a *gradual* transition occurs from a normal state to a dimerized one. One should emphasize the main difference between the real ground state and its quasidegenerate mate and the two degenerate MF ground states in the dimerized regime. The former could be only approximately considered as the symmetric and antisymmetric combinations of the latter. In reality, the two contributions cannot be separated in the exact states. The closer to the critical point the more pronounced is this nonseparability. We have also computed the critical curve $\lambda(\Omega_0)$ by using the wave function $|\Psi_{CA}\rangle \equiv (|\Psi_{CAA,+}\rangle + |\Psi_{CAA,-}\rangle)/\sqrt{2}$ as an approximation for the true ground state. As seen in Figure 2a, this crude treatment accounts only qualitatively for quantum phonon fluctuations.

5.2 Lattice excitation energies: an alternative way of revealing the gradual transition

The examination of the frequencies of lattice excitations, to which this section is devoted, will offer an alternative approach to the smooth transition. Within RPA (*cf.* Eqs. (3, 4)), the phonon frequency gradually decreases from Ω_0 to 0, as λ increases from 0 to λ_c^{MF} (Fig. 3). This agrees with the idea that a soft mode instability of the normal state drives the system towards a dimerized state (*e.g.* Ref. [11]). In the dimerized state, $\Omega \neq 0$: the phasons of a commensurate CDW are pinned [11].

In Figure 3, the RPA-frequencies can be compared with the exact frequencies $\Omega_{1,e}$ and $\Omega_{2,e}$ (*cf.* Sect. 4.2). Ω_{RPA} represents a good approximation for $\Omega_{1,e}$ in the weak coupling limit ($\lambda \ll \lambda_c^{MF}$), while it becomes close to $\Omega_{2,e}$ in the strong coupling limit ($\lambda \gg \lambda_c^{MF}$). The reasons for this behavior will be clarified below.

For λ sufficiently smaller than λ_c^{MF} and for low enough Ω_0, the exact results agree with the physics emerging from the MF-RPA picture. The curves $\Omega_{1,e}$ and $\Omega_{2,e}/2$, being very close to each other and also to the Ω_{RPA}-curve, show that the lattice excitations are normal, almost harmonic phonons (Fig. 3) and support the conclusion of Section 5.1.

Increasing λ toward λ_c^{MF}, the difference between $\Omega_{1,e}$ and Ω_{RPA} becomes more and more pronounced. The $\Omega_{1,e}$-curve exhibits an overall softening. Nevertheless, at variance with the complete phonon softening of the Ω_{RPA}-curve ($\Omega_{RPA}(\lambda_c^{MF}) = 0$), this softening is never complete for finite Ω_0. For $\lambda > \lambda_c^{MF}$, $\Omega_{1,e} \propto \exp(-23.5\Omega_0^{-0.7}\lambda)$ for $0.01 < \Omega_0 < 1$. $\Omega_{2,e}$ behaves differently for small and large λ (Fig. 3). For small λ, $\Omega_{2,e}$ becomes softer with increasing λ. Simultaneously, the anharmonicity becomes progressively stronger: the curves $\Omega_{1,e}$ and $\Omega_{2,e}/2$ gradually depart from each other. Besides, the anharmonicity increases with increasing Ω_0. By further increasing λ, an upturn appears in the $\Omega_{2,e}$-curve at a certain value $\lambda = \lambda_u$ ($= 0.50$ at $\Omega_0 = 0.5$). Unlike its Ω_0-independent MF-RPA counterpart λ_c^{MF}, λ_u increases with Ω_0. For $0.01 < \Omega_0 < 1$, we found $\lambda_u = \lambda_c^{MF} + 0.19\Omega_0^{2/3}$ and $\Omega_{2,e}|_{\lambda=\lambda_u} = 0.58\Omega_0^{4/3} = 16.6(\lambda_u - \lambda_c^{MF})^2$.

Increasing λ beyond λ_u, $\Omega_{1,e}$ approaches 0, whereas $\Omega_{2,e}$ increases monotonically (Fig. 3) and behaves qualitatively similar to Ω_{RPA}. The MF-RPA results can be expressed as follows. The tunneling between the wells at $+\mathcal{Q}_{MF}$ and $-\mathcal{Q}_{MF}$ requires no energy because the corresponding states are degenerate, while the energy cost for a proper lattice excitation is Ω_{RPA}. This picture represents a reasonable approximation ($\Omega_{1,e} \approx 0$, $\Omega_{2,e} \approx \Omega_{RPA}$) only for a coupling sufficiently stronger than λ_c^{MF} and low Ω_0.

In summary, the RPA results have physical sense either in the weak or strong coupling limit but are meaningless in the critical region. This reveals the limitation of the description based on two independent states associated with the two wells of $V_0(Q)$ already discussed in Section 5.1. $\lambda_u(\Omega_0)$ could alternatively define the dimerization onset.

5.3 Validity of AA description

The exact and AA results almost coincide within the drawing accuracy of Figures 1 and 3 even at relatively large Ω_0. The largest differences occur in the critical region. Although the difference between exact and AA results for λ_c becomes larger at higher frequencies (Fig. 2a) it remains significantly smaller than their difference from λ_c^{MF}. AA remains reliable up to rather high Ω_0-values (Figs. 2a, b).

For subsequent applications to mesoscopic systems, it is highly desirable to assess the AA validity self-consistently rather than comparing AA and exact results.

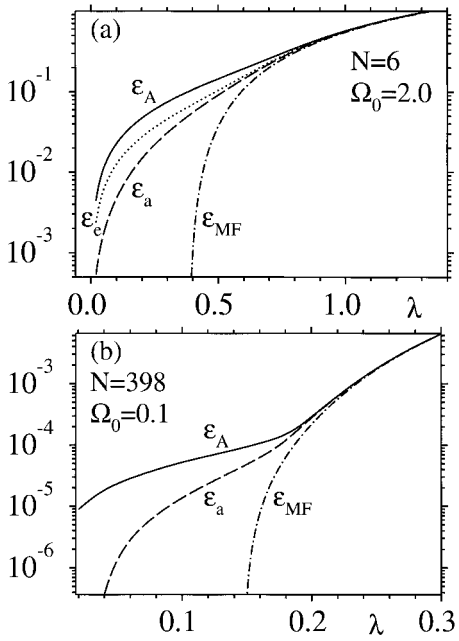

Fig. 4. Condensation energy per site computed exactly (ε_e) and within AA without (ε_A) and with (ε_a) diagonal correction and within MF (ε_{MF}). Note the logarithmic scale.

To this aim, we shall examine now the AA diagonal corrections (*cf.* Sect. 4.1 and Ref. [3]). For $N = 6$, we have computed the condensation energy per site both exactly (ε_e) and within AA, in the latter case without (ε_A) and with (ε_a) diagonal corrections [$N\varepsilon_\mu \equiv V_0(Q)|_{Q=0} - E_\mu$; $\mu = e, A, a$]. Figure 4a illustrates a typical situation. For couplings stronger than a certain value (that increases with Ω_0), AA is excellent: the stronger the coupling, the better the AA description. The ε_e-, ε_A- and ε_a-curves progressively depart from each other [17] for decreasing λ. However, $|\varepsilon_e - \varepsilon_a| < |\varepsilon_A - \varepsilon_a|$, indicating that the AA wave functions are accurate even for couplings weaker than those suggested by comparing ε_A and ε_a. This conclusion is also supported by comparing exact and AA values of $\Omega_{1,2}$ and η (*cf.* Fig. 3 and 2b). Thus, one can state that AA describes sufficiently reliable the critical region even at rather high frequencies Ω_0.

6 Mesoscopic systems

In this section we shall present results on the Peierls transition in systems with variable sizes N. Expressing alternatively a MF-result of Section 3, only chains larger than a certain critical size $N_c^{MF}(\lambda)$ are dimerized. If the coupling is reasonably weak, the Peierls transition is strongly size dependent in mesoscopic systems even at the MF level, see Figure 5a.

The AA results collected in Figures 5 and 6 show that the quantum phonon fluctuations are quite important at small coupling. The critical size N_c for dimerization onset as discussed in Section 5.1 is much larger than N_c^{MF} even

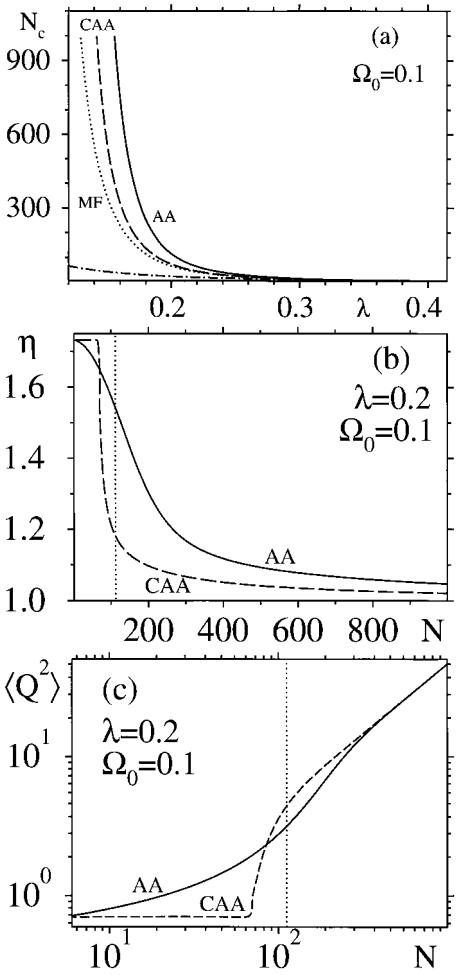

Fig. 5. (a) λ-dependence of the critical size N_c for dimerization at $\Omega_0 = 0.1$ predicted within MF, AA and CAA. The dot-dashed line was computed by imposing $2t\sin(\pi/N) = \Delta_{MF}$. (b, c) The smooth Peierls transition as illustrated by η- and $\langle Q^2\rangle$-curves. ($N_c = 112$ is marked by vertical dotted lines.)

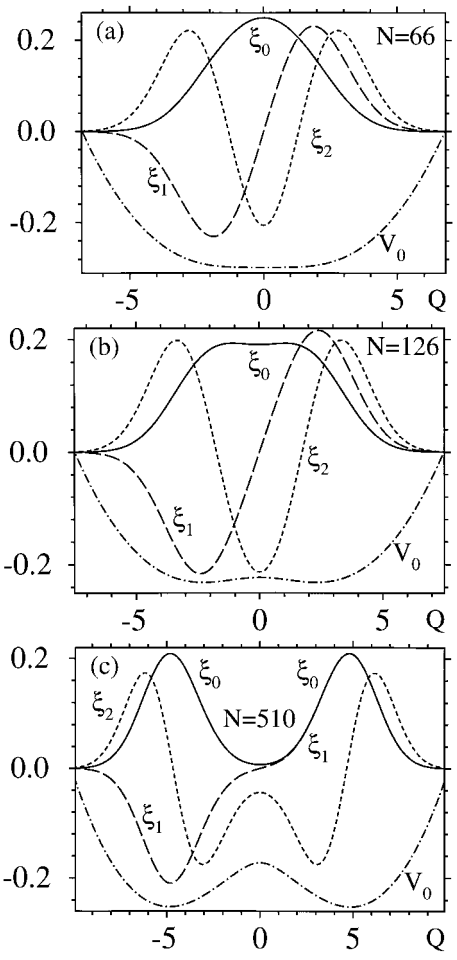

Fig. 6. The same as in Figure 1, for $\lambda = 0.2$ and $\Omega_0 = 0.1$ and three different N-values.

for small Ω_0 ($N_c = 112$, $N_c^{MF} = 66$ for $\Omega_0 \sim 0.1t$, see Fig. 5a).

The transition region is very broad. This is illustrated by the parameter η which interpolates smoothly between the values $\sqrt{3}$ and 1 characterizing ideal normal and dimerized states, respectively (Fig. 5b). Figure 5c illustrates the same behavior: $\langle Q^2\rangle$ evolves slowly from the value 0.5 expected for normal phonons to a value proportional to N, as expected for condensed phonons. The difference between AA and CAA results is very clear, particularly in the transition region. The smooth variation displayed by the AA curves indicates that a well defined dimerized state should be expected at sizes significantly larger than N_c. This fact makes the difference from the MF picture even more important.

AA also allows to monitor the changes occurring with increasing size by inspecting the wave functions. At $\lambda = 0.2$ the chain with 66 sites is extremely close to the MF critical point ($\lambda_c^{MF} = 0.1997$). The two minima of $V_0(Q)$ are very shallow and, therefore, the ground state wave function $\xi_0(Q)$ displays a single maximum (Fig. 6a), *i.e.* it is of normal type. At the same λ, two symmetric maxima are hardly visible in $\xi_0(Q)$ for $N = 126$ ($\gtrsim N_c = 112$) (Fig. 6b). With increasing size, the two maxima become more and more well separated, as seen in Figure 6c for $N = 510$. Figures 1 and 6 show two ways in which a system can be driven from a normal state towards a dimerized one: by increasing the coupling λ or the size N. The modifications do not only refer to the ground state $\xi_0(Q)$: the lowest excited states $\xi_{1,2}(Q)$ are also changed accordingly.

To check the accuracy of the AA results for mesoscopic systems we have computed the AA diagonal corrections. They behave similar to those for small systems (*cf.* Figs. 4a and b). We have also estimated how inaccurate the AA prediction on the critical point could be. The study on 6-site chains turned out to be helpful to this aim, too. For $N = 6$ and various Ω_0 we have inspected the values λ_u^A and λ_u^a at the minimum of $\Omega_{2,A}(\lambda)$ and $\Omega_{2,a}(\lambda)$ (*cf.* Sect. 5.2). $\lambda_u^A - \lambda_u^a$ is very close to the difference between the AA and exact values of λ_c. Using $\lambda_u^A - \lambda_u^a$ to estimate the inaccuracy of AA, we claim an overestimation of $\lambda_c - \lambda_c^{MF}$ by at most 25% (5%) for $N < 1000$ ($N < 100$).

7 Summary and outlook

The results on finite Peierls chains reported above mainly comprise three aspects. First, we have developed a method (AA) that can describe quantitatively the structural change occurring in chains up to mesoscopic sizes. We extend the conclusion [3] obtained for chains with $N = 4n$: AA is much less restrictive than textbooks usually claim for adiabatic approximations. The AA-results are accurate *at least* when the diagonal corrections are small. The magnitude of the latter turned out to be more appropriate for assessing self-consistently the validity of AA than the ratio κ of the electronic gap to the phonon frequency. Contrary to textbook wisdom, we have found that AA is applicable even if $\kappa \sim 1$.

Second, the quantum phonon fluctuations yield a *smooth* Peierls transition in finite chains, in contrast to the sharp MF transition. The ground state wave function does preserve the symmetry of the original Hamiltonian. There is no symmetry breaking in *finite* Peierls chains. In infinite systems, the two states related to the deep wells at $+\mathcal{Q}_{MF}$ and $-\mathcal{Q}_{MF}$ of the adiabatic potential are degenerate and independent of each other. In finite chains, the contributions of these wells cannot be separated because of the nonnegligible transmission coefficient of tunneling [18]. This explains why the MF and RPA methods poorly describe the dimerization in finite chains, particularly close to the dimerization onset (see Figs. 3 and 4). They assume that the contributions of the two wells can be separated. The closer to the critical region, the poorer is the approximation of independent wells. In infinite systems quantum phonon fluctuations are often accounted for by including one-loop correction to the order parameter. We checked that this method is also poor in finite chains [19], a fact understandable since it starts by an expansion around a *single* minimum. For a given λ (or N), the dimerization develops in chains with sizes (or couplings) larger than a critical value N_c(or λ_c). N_c increases with Ω_0 and is significantly larger than N_c^{MF}. The critical region is very broad; a well defined dimerization exists only for sizes considerably larger than N_c.

Third, this effect could be observable in materials with weak electron-phonon coupling. For $\lambda \approx 0.15 - 0.2$ ($2\Delta_{MF}/t \approx 0.02 - 0.11$), the Peierls dimerization of infinite chains should disappear for sizes smaller than $N \approx 4000{-}300$ at $\Omega_0/t \simeq 0.1$. The larger Ω_0 and especially (*cf.* Fig. 5a) the smaller λ, the easier is the experimental observation. In addition, various interchain interactions could enhance this effect.

We suggest two experimental techniques to study the smooth structural change in Peierls chains, namely nonlinear optical absorption and ultrasound attenuation. The latter could reveal the strong anharmonicity in the critical region. The former technique can be used for directly probing the symmetry [19]. In the normal regime, temperatures sufficiently lower than Ω_1 exist, where one- and three-photon processes can cause transitions of electrons from the (symmetric) ground state across the Peierls gap (G), while two-photon processes are forbidden by symmetry. In the critical or dimerized regime, Ω_1 is very small and the first excited state is also populated. Because it is antisymmetric, transitions from this state across the Peierls gap *via* two-photon processes become possible. Therefore, besides the maximum at $\omega \sim G/3$, a maximum of the nonlinear absorption should progressively develop at a frequency $\omega \sim G/2$ as one moves from the normal regime to the dimerized one; G can be extracted from the maximum of the linear optical absorption.

How small a superconductor can be was considered to be a fundamental theoretical question [10]. There, the discrete electron energy-level spectrum has been predicted to change the properties even to the point of extinguishing superconductivity altogether [10,20]. Recent experiments on nanometer-scale metal particles seem to confirm this expectation [20]. Existing theoretical investigations within MF predict that the superconductivity is lost when the average spacing in the discrete energy spectrum of the finite superconductor is of the order of the BCS order parameter [10,20]. We have computed a critical curve by imposing a similar condition [$2t \sin(\pi/N) = \Delta_{MF}$] for the present model. These critical sizes are much smaller than those obtained both within MF and by accounting for quantum phonon fluctuations (Fig. 5a). Whether the notable difference is due to the enhanced fluctuation effect in one dimension or whether quantum fluctuations should also quantitatively change the estimated minimum size of three-dimensional superconductors remains to be clarified.

In annulene $C_{4n+2}H_{4n+2}$, the Hückel approach (basically, a MF-approach to the Su-Schrieffer-Heeger (SSH) model) predicted a minimum size $4n+2 \gtrsim 18-30$ for bond alternation, such that only small molecules (like benzene) possess equivalent chemical bonds [9]. Since that approach ignored the quantum fluctuations, the critical size could be significantly underestimated. The AA method can be applied to the SSH model without difficulty.

To the best of our knowledge, no experimental study previously revealed that a minimum size is required for a Peierls dimerization and no previous theoretical investigation suggested that, because of quantum phonon fluctuations, this minimum size could be large enough to be observed in mesoscopic systems. We hope that the present theoretical study will also stimulate a similar experimental interest on mesoscopic Peierls systems.

The authors thank the Sonderforschungsbereich 247 at the Universität Heidelberg and the Sonderforschungsbereich 195 at the Universität Karlsruhe (I. B.) for financial support and the referee for useful suggestions concerning the presentation. We dedicate this paper to Professor G. Huttner on the occasion of his 60th birthday.

References

1. See, *e.g.*, *Transport Phenomena in Mesoscopic Systems* edited by H. Fukuyama, T. Ando (Springer-Verlag Berlin, 1992); *Quantum Dynamics of Submicron Structures*, edited by H.A. Cerdeira, B. Kramer, G. Schön, NATO ASI Series E, vol. 291 (Kluwer, 1995).

2. H.S.J. van der Zant, *et al.*, Synth. Metals **86**, 1781 (1997).
3. I. Bâldea, H. Köppel, L.S. Cederbaum, Phys. Rev. B **55**, 1481 (1997).
4. C.Q. Wu, Q.F. Huang, X. Sun, Phys. Rev. B **52**, 15683 (1995); Q.F. Huang, C.Q. Wu, X. Sun, Phys. Rev. B **52**, 5637 (1995).
5. K. Nasu, J. Phys. Soc. Jpn **54**, 1933 (1985); H. Zheng, D. Feinberg, M. Avignon, Phys. Rev. B **39**, 9405 (1989); H. Zheng, Phys. Rev. B **50**, 6717 (1994); X. Wang, H. Zheng, Phys. Rev. B **52**, 15261 (1995).
6. E. Fradkin, J.E. Hirsch, Phys. Rev. B **27**, 1680 (1983); *ibid.* **27**, 4302 (1983).
7. R. Fehrenbacher, Phys. Rev. B **49**, 12230 (1994); G.-P. Borghi, *et al.*, Europhys. Lett. **34**, 127 (1996).
8. S. Weber, H. Büttner, Solid St. Commun. **56**, 395 (1985); V. Waas, H. Büttner, J. Voigt, Phys. Rev. B **41**, 9366 (1990); B.S. Shastry, B. Sutherland, Phys. Rev. Lett. **65**, 243 (1990); J. Wagner, W. Hanke, D.J. Scalapino, Phys. Rev. B **43**, 10517 (1990); R.M. Fye, *et al.*, Phys. Rev. B **44**, 6909 (1991).
9. See, *e.g.* W. Kutzelnigg, *Einführung in die Theoretische Chemie*, vol. 2, ch. 11 (Verlag Chemie, Weinheim-New-York, 1978) (in German).
10. P.W. Anderson, J. Phys. Chem. Solids **11**, 28 (1959).
11. G. Grüner, *Density Waves in Solids* (Frontiers of Physics Series, Addison-Wesley Massachusetts, 1994).
12. This is the case in (anti)periodic chains with $N = 4n + 2$ ($N = 4n$). By contrast, one has $\mathcal{Q}_{MF} \neq 0$ for any $\lambda > 0$ in (anti)periodic chains with $N = 4n$ ($N = 4n + 2$).
13. C.J. Ballhausen, A.E. Hansen, Ann. Rev. Phys. Chem. **23**, 15 (1972); H.C. Longuet-Higgins, Adv. Spectrosc. **2**, 429 (1961).
14. See, *e.g.*, H. Köppel, W. Domcke, L.S. Cederbaum, Adv. Chem. Phys. **57**, 59 (1984).
15. To get the Q-distribution one should perform the transformation from the ν- to the Q-basis.
16. G. Herzberg, *Infrared and Raman Spectra of Polyatomic Molecules* (Van Nostrand Reinhold, New York, 1945).
17. The inequality $E_A < E_e$ ($\varepsilon_A > \varepsilon_e$) does not contradict the variational principle: E_A is not an expectation value (but a certain approximate eigenvalue) of the Hamiltonian.
18. The transmission coefficient
$$\exp\left(-\mathcal{Q}_{MF}\sqrt{\left[V_0(0) - V_0(\mathcal{Q}_{MF})\right]/\Omega_0}\right)$$
and Ω_1 significantly differ from 0 in the same parameter region.
19. I. Bâldea, H. Köppel, L.S. Cederbaum, (unpublished).
20. C.T. Black, D.C. Ralph, M. Tinkham, Phys. Rev. Lett. **76**, 688 (1996); D.C. Ralph, C.T. Black, M. Tinkham, *ibid.* **74**, 3241 (1995); R.A. Smith, V. Ambegaokar, *ibid.* **77**, 4962 (1996); J. van Delft, *et al.*, *ibid.* **77**, 3189 (1996); F. Braun, *et al.*, *ibid.* **79**, 921 (1997).